

Multi-Frequency Study of the B3–VLA Sample. I. 10.6-GHz Data

L. Gregorini^{1,2}, M. Vigotti¹, K.-H. Mack^{1,3}, J. Zönnchen³, and U. Klein³

¹ Istituto di Radioastronomia del CNR, Via Gobetti 101, I-40129, Bologna, Italy

² Dipartimento di Fisica, Università di Bologna, Via Irnerio 46, I-40126, Bologna, Italy

³ Radioastronomisches Institut der Universität Bonn, Auf dem Hügel 71, D-53121 Bonn, Germany

August 1998

Abstract. We present radio continuum data for 1050 B3 radio sources at 10.6 GHz. These sources constitute the B3-VLA sample which is complete down to 100 mJy at 408 MHz. The aim is the construction of a homogeneous spectral database for a large sample of radio sources, 10 times fainter than the Kühn et al. (1981) sample, in the range 151 MHz to 10.6 GHz. Extended and complex radio sources (53) were mapped; the remaining ones were observed with cross-scans. We detected 99% of the radio sources with a flux density error of about 1 mJy for the fainter ones. The analysis of the quality of the 10.6 GHz data is presented.

Key words: Radio continuum: general – Galaxies: general – Quasars: general

1. Introduction

The study of large samples of radio sources over a frequency range as wide as possible is still an important branch of modern astrophysics because of its cosmological relevance. While early radio surveys naturally discovered strong sources (many of which are also intrinsically luminous), the need for surveys of intermediate or low flux densities became apparent. One important radio survey aiming at lower source flux densities was the so-called B3 survey (Ficarra et al. 1985), carried out at 408 MHz and complete down to 100 mJy at that frequency and naturally delivering a huge number of radio sources, in this case 13354. A subsample of 1050 sources was later observed with the VLA (hereafter B3-VLA sample; Vigotti et al. 1989), the selection criterion ensuring roughly equal numbers of sources in 5 flux density intervals. Measurements of 429 sources at 1.4 GHz and of 770 sources at 4.75 GHz

Send offprint requests to: L. Gregorini, Istituto di Radioastronomia del CNR, Via Gobetti 101, I-40129, Bologna, Italy

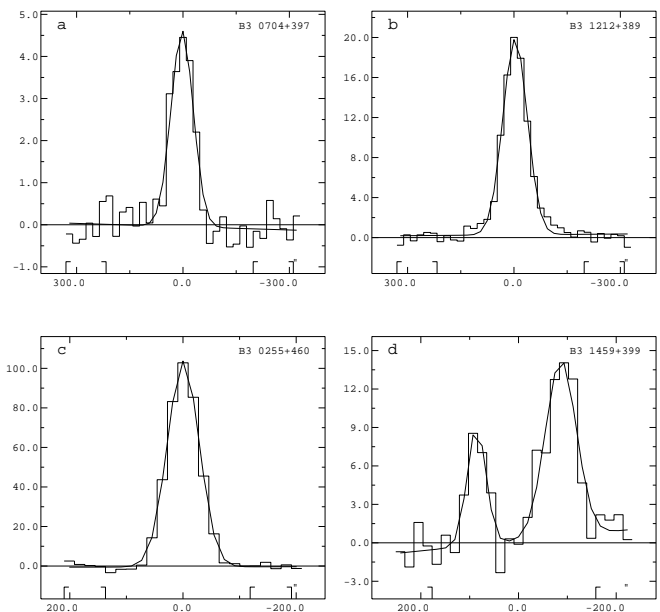


Fig. 1. Examples of cross-scans at $\lambda 2.8$ cm: a) a 4 mJy source, b) a 20 mJy source, c) a 100 mJy source, d) a double source

were conducted by Kulkarni et al. (1990). Based on these surveys the spectral properties and their possible spectral evolution has been investigated and discussed (e.g. Kulkarni & Mantovani 1985; Kapahi & Kulkarni 1986).

Our aim is the construction of a homogeneous spectral database for a large radio sources sample 10 times fainter than that of Kühn et al. (1981). The 6C survey (Hales et al. 1988) contributes the 151-MHz flux density, the WENSS (Rengelink et al. 1997) the 327-MHz flux density. The 408-MHz flux density is taken from the B3 survey (Ficarra et al. 1985) while the NVSS (Condon et al. 1998) yields the 1400-MHz flux density. The GB6 survey (Gregory et al. 1996) combined with the work of Kulkarni et al. (1990) provides the 4.75 GHz flux densities for 80% of the B3-VLA sample.

Table 1. B3 VLA sources at 10.6 GHz (cont'd)

B3 name	RA (B1950) [h m s]	DEC (B1950) [° ′ ″]	S _{peak} [mJy]	S _{int} [mJy]	ID	B3 name	RA (B1950) [h m s]	DEC (B1950) [° ′ ″]	S _{peak} [mJy]	S _{int} [mJy]	ID
0827+458	08 27 07.3	45 53 36	45.8	47.5		0944+390B	09 44 23.6	39 00 46	15.2	15.2	g
0828+381	08 28 35.8	38 06 43	17.7	18.7	g	0944+397	09 44 44.8	39 47 07	4.6	4.6	
0829+395	08 29 58.3	39 31 34	29.5	29.5		0945+408	09 45 50.1	40 53 43	1391.5	1391.5	Q
0829+425	08 29 26.4	42 35 13	135.1	135.1	Q	0945+419	09 45 23.7	41 55 41	39.7	41.0	
0831+393	08 31 38.4	39 21 13	15.4	15.4		0947+405	09 47 23.7	40 31 59	16.4	16.4	
0831+399	08 31 16.3	39 55 13		16.7		0947+424	09 47 11.8	42 27 00	60.2	60.2	
0832+395	08 32 14.6	39 33 09	36.2	36.2		0948+390	09 48 58.6	39 04 38	15.4	15.4	g
0832+399	08 32 21.8	39 55 04	5.4	5.7		0950+402	09 50 59.1	40 14 02	12.0	13.1	
0834+399	08 34 08.9	39 57 53	7.8	7.8		0951+398	09 51 27.3	39 52 11	15.0	15.0	g
0834+450A	08 34 27.1	45 00 54		301.3	g	0951+408	09 51 39.2	40 50 57	32.7	34.1	Q
0836+399	08 36 55.2	39 54 29	7.8	7.8		0951+422	09 51 07.0	42 15 19	110.3	110.3	g
0836+402	08 36 54.3	40 14 38	84.5	84.5	g	0953+382	09 53 43.4	38 17 19	28.9	28.9	
0836+426	08 36 35.6	42 38 33	207.5	207.5	Q	0953+398	09 53 05.9	39 49 31	129.0	129.0	Q
0837+399	08 37 51.4	39 55 30	5.7	6.2		0954+436	09 54 39.2	43 41 08	51.0	51.0	Q
0838+396	08 38 54.6	39 37 58	8.1	8.1		0955+380	09 55 30.4	38 01 37	11.1	11.1	
0840+400	08 40 50.5	40 03 53	2.4	2.4		0955+387	09 55 01.6	38 44 19	44.0	46.1	Q
0840+424A	08 40 11.5	42 26 20	272.0	272.0		0955+390	09 55 42.9	39 02 44	58.9	58.9	
0841+386	08 41 14.8	38 41 49	245.1	245.1		0955+396	09 55 55.0	39 36 52	17.9	17.9	
0841+397	08 41 06.0	39 45 03		<3		0956+391	09 56 42.4	39 11 26	12.3	12.3	
0841+403	08 41 39.4	40 19 09	46.5	54.6	g	0956+404	09 56 34.8	40 29 52	7.1	7.1	
0841+407	08 41 51.5	40 42 12	35.0	38.0		0956+475	09 56 08.0	47 35 37	29.9	29.9	G
0842+401	08 42 47.6	40 07 55	21.1	22.7		0957+399	09 57 44.4	39 55 12	4.3	4.3	
0843+425	08 43 59.0	42 34 42		51.1	g	0958+390A	09 58 23.8	39 02 24	15.8	15.8	
0844+396	08 44 35.5	39 41 06	7.3	7.3		0958+391	09 58 17.7	39 06 14	2.8	2.9	
0847+406	08 47 24.8	40 40 28	12.8	12.8		1004+446	10 04 14.3	44 39 53	141.9	168.1	
0849+394	08 49 24.9	39 30 26	5.4	6.2		1007+417	10 07 26.1	41 47 16	323.1	335.3	Q
0849+424	08 49 15.6	42 26 47	57.3	57.3	Q	1007+422	10 07 22.8	42 14 19	72.7	72.7	
0850+383	08 50 41.3	38 22 39	12.0	12.0		1008+395	10 08 56.2	39 34 54	8.3	8.3	
0852+384	08 52 43.2	38 25 03	24.0	24.4		1008+423	10 08 53.5	42 19 23	101.4	101.4	
0854+399B	08 54 29.0	39 57 12	70.9	70.9	G	1008+467A	10 08 39.3	46 43 09	92.8	92.8	G
0855+397	08 55 02.1	39 42 33	3.8	4.5		1009+389A	10 09 26.0	38 58 56	16.8	16.8	
0855+419	08 55 44.0	41 54 59	25.4	25.4		1009+434	10 09 07.0	43 27 55	9.2	9.2	G
0856+397	08 56 25.4	39 42 04	9.6	10.2		1012+389	10 12 59.2	38 56 50	18.9	18.9	
0856+406	08 56 45.1	40 36 18	10.4	10.4	G	1012+395	10 12 52.6	39 35 04	8.4	9.2	
0857+391	08 57 41.7	39 07 59	82.6	86.4	g	1012+425	10 12 31.5	42 34 45	22.0	23.6	
0857+402	08 57 15.9	40 16 43	22.4	22.4		1013+410	10 12 58.2	41 01 46		186.3	g
0858+386	08 58 20.8	38 38 59	58.0	58.0		1014+392	10 14 16.5	39 16 23	228.6	228.6	g
0858+388	08 58 03.0	38 53 55	10.5	10.5		1014+397A	10 14 19.5	39 46 32		112.0	g
0858+452	08 58 54.7	45 12 43	104.2	104.2		1015+383	10 15 29.0	38 20 30	61.5	65.9	Q
0859+470	08 59 39.9	47 02 56	933.4	933.4	Q	1016+388B	10 16 50.5	38 48 40	18.0	19.3	
0900+380B	09 00 49.8	38 04 28	15.5	16.0		1016+396	10 16 29.5	39 37 45		<3	
0900+389	09 01 00.3	38 58 26		23.5		1016+397	10 16 57.5	39 45 25	9.4	9.4	g
0900+395	09 00 13.4	39 30 35	5.9	9.0		1016+443	10 16 46.5	44 23 30	21.1	21.1	g
0900+428	09 00 58.8	42 50 02	450.9	450.9	g	1018+393	10 18 41.1	39 19 03	10.3	10.3	
0902+383	09 02 17.7	38 19 26	27.6	28.3		1018+405	10 18 47.1	40 34 48	20.2	20.7	
0902+384	09 02 02.5	38 26 34	11.0	11.0		1019+382A	10 19 27.2	38 18 02	39.5	39.5	
0902+414	09 02 48.0	41 28 31	132.7	132.7	g	1019+394	10 19 58.7	39 24 00	45.4	45.4	G
0902+416	09 02 07.2	41 40 39	103.8	103.8		1019+395	10 19 18.8	39 32 39	8.4	8.4	
0903+428	09 03 09.7	42 51 08	26.8	26.8		1019+397	10 19 41.3	39 47 01	25.3	26.6	
0904+386	09 04 34.9	38 39 46	27.0	27.0	Q	1020+400	10 20 14.6	40 03 28	852.1	852.1	Q
0904+396	09 04 26.8	39 36 36	5.6	6.0		1021+384	10 21 00.9	38 24 00	40.9	40.9	Q
0904+399	09 04 15.5	39 56 26	36.1	36.1	g	1022+432	10 22 30.6	43 12 58	76.0	76.0	
0904+417B	09 04 18.4	41 46 49	126.9	200.2	g	1023+393	10 23 08.6	39 20 39	16.2	16.2	g
0905+380A	09 05 41.3	38 00 29	158.4	161.2	G	1024+463	10 24 13.3	46 18 09	113.9	214.7	G
0905+399	09 05 05.8	39 55 24	16.9	16.9	G	1025+390B	10 25 49.4	38 59 57	220.3	220.3	g
0906+383	09 06 53.3	38 18 31	20.4	20.4		1025+394	10 25 55.9	39 26 08	12.6	12.6	
0906+421	09 06 30.8	42 09 33	4.5	4.6		1027+383	10 27 46.3	38 18 46	32.0	32.0	
0906+430	09 06 17.3	43 05 59	1128.4	1128.4	Q	1027+390	10 27 31.7	39 02 25	11.3	12.1	
0907+381	09 07 45.0	38 11 32	106.9	106.9	Q	1027+392	10 27 21.7	39 13 18	80.7	80.7	
0908+380B	09 08 39.6	38 02 37	26.3	26.3	G	1028+400	10 28 21.8	40 02 21	19.8	19.8	
0908+380C	09 08 54.0	38 03 54	103.2	108.7	G	1028+402	10 28 07.4	40 16 09	26.0	26.0	
0909+395	09 09 30.0	39 35 07	6.0	6.0		1030+398	10 30 27.5	39 51 20	382.3	382.3	G
0909+432	09 09 44.9	43 17 44	36.1	36.1		1030+415	10 30 07.8	41 31 34	230.3	230.3	Q
0910+392	09 10 41.6	39 14 35	19.2	19.2	Q	1033+387A	10 33 30.3	38 47 07		21.5	g
0911+384	09 11 27.9	38 29 10	29.7	29.7		1033+387B	10 33 52.8	38 42 19	7.9	8.1	
0911+395	09 11 28.1	39 35 08	16.0	16.0		1033+388	10 33 41.8	38 51 07		31.8	g
0911+418	09 11 32.2	41 49 36	114.2	114.2	g	1033+408	10 33 31.3	40 51 01	25.3	27.0	
0912+388	09 12 25.0	38 50 26	15.1	15.1		1034+397	10 34 40.5	39 43 36	5.7	6.6	
0912+392	09 12 55.5	39 12 51	7.2	7.2	Q	1034+404	10 34 18.3	40 27 13	84.0	84.0	G
0913+385	09 13 39.3	38 30 41	59.5	62.7	Q	1035+398	10 35 23.5	39 48 32	16.9	16.9	
0913+391	09 13 39.5	39 07 02	487.0	487.0	Q	1037+399	10 37 19.2	39 58 06		8.6	
0914+390	09 14 32.7	39 01 54	6.9	8.7		1038+398	10 38 36.5	39 49 38	16.5	16.5	
0917+458A	09 17 50.4	45 51 47		1279.0	Q	1039+397	10 39 08.7	39 42 41	47.9	49.3	
0918+381	09 18 38.8	38 06 56	90.3	113.7	g	1039+424	10 39 11.8	42 26 13	23.2	23.2	
0918+395	09 18 24.6	39 30 31	10.5	11.1	g	1040+395	10 40 13.2	39 30 00	50.3	50.3	
0918+444	09 18 15.8	44 26 33	84.6	84.6	g	1040+397	10 40 25.3	39 45 22	8.5	8.5	
0919+381	09 19 08.0	38 06 52	27.9	27.9	G	1040+398	10 40 43.8	39 49 57	8.5	9.3	g
0920+390	09 20 06.3	39 02 32	299.0	299.0		1041+392	10 41 34.5	39 16 36	30.3	30.3	
0920+408	09 20 52.4	40 47 54	50.8	53.5	g	1042+392	10 42 23.6	39 12 25	87.8	87.8	
0921+400	09 21 40.8	40 03 27	20.7	20.7		1042+393	10 42 29.7	39 20 06	7.3	8.4	
0922+397	09 22 44.1	39 48 06	2.4	2.4		1042+397	10 42 48.6	39 45 56	27.1	27.1	
0922+407	09 22 50.7	40 42 49	326.6	326.6	Q	1043+394	10 43 06.4	39 28 55	13.3	14.2	
0922+422	09 22 47.8	42 16 35	20.9	20.9	Q	1044+454	10 44 38.6	45 24 43	23.6	23.6	
0922+425	09 22 11.9	42 30 26	30.5	30.5	Q	1047+387	10 47 56.0	38 47 43	28.5	28.5	
0923+392	09 23 55.3	39 15 24	12040.8	12040.8	Q	1047+396	10 47 23.1	39 41 37	5.9	5.9	
0923+398	09 23 38.3	39 50 47	75.6	75.6	Q	1049+384	10 49 22.3	38 27 39	71.2	71.2	
0926+388	09 26 34.5	38 49 12	10.8	10.8		1050+391	10 50 44.2	39 09 46	18.7	18.7	
0926+392	09 26 08.4	39 12 23	12.8	12.8		1052+380	10 52 56.1	38 02 02	10.7	10.7	
0929+395	09 29 18.2	39 31 52	19.0	19.0		1052+389	10 52 36.0	38 56 19	4.5	4.8	
0930+389	09 30 00.7	38 55 10	26.3	26.3	G	1053+384	10 53 23.9	38 24 45	42.1	52.4	
0930+395	09 30 35.0	39 35 10	25.7	26.8		1053+394	10 53 59.8	39 27 28	15.3	16.4	</

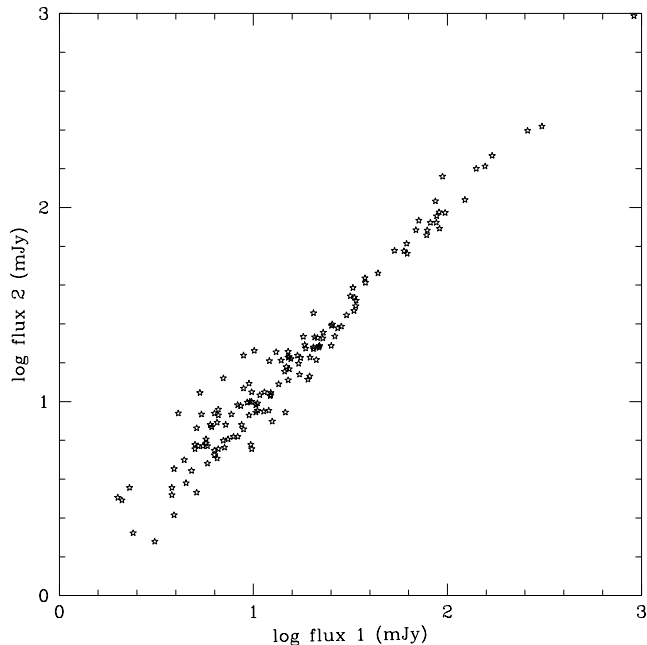


Fig. 2. Plot of flux densities measured at two different epochs.

We have therefore embarked on a project to survey the entire sample at 10.6 GHz (i.e. $\lambda 2.8$ cm) using the Effelsberg 100-m telescope. Since all measurements were carried out using IF polarimeters we have information about the linear polarization of a large number of sources, which will be reported at a later stage.

In Sect. 2 we describe the observing techniques and data reduction. Section 3 presents the results.

2. Observations and data reduction

The observations reported here were carried out between May 1994 and January 1996. The 4-feed receiver system installed in the secondary focus of the 100-m telescope was used in a multi-beam mode. Each horn feeds a 2-channel receiver with an IF polarimeter providing full Stokes information simultaneously. The system temperature was ~ 80 K on the sky (zenith), the effective bandwidth was 300 MHz. In the beginning of 1995 the receiver's band centre had to be moved from 10.55 GHz to 10.45 GHz in order to avoid the new ASTRA 1D satellite. This is only a change of 1% in frequency, which will not have any noticeable influence on the observed source properties (for a source with spectral index $\alpha = -1$ this implies a 1% change in flux density; $S_\nu \sim \nu^\alpha$). The nominal half-power beam width is $69''$. The total number of sources observed was 1050.

2.1. Cross-Scans

Almost all the sources (95%) were observed with cross-scans, with the main beam scanning a distance of $7'$ to ensure adequate baselines. The scanning speed was $30'/\text{min}$.

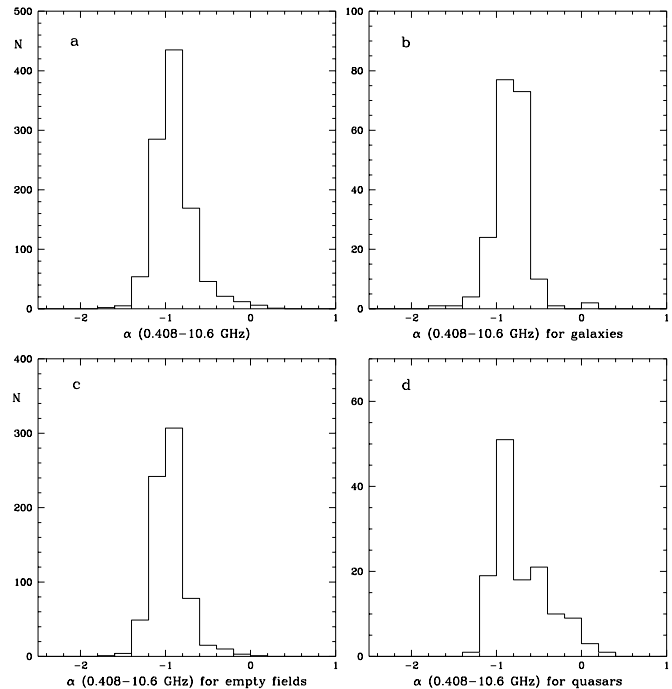


Fig. 3. Histograms of spectral indices between 408 MHz and 10.6 GHz. a) for the whole sample, b) for POSS-I galaxies, c) for empty fields, and d) for quasars (see text).

The offset feeds were used to efficiently remove atmospheric noise. For sources less extended than $30''$ the cross-scans were oriented in right ascension and declination. In the case of more extended sources, the cross-scans were oriented with one scan direction along the sources' major axes (e.g. along double or triple components), with the scan length increased to $10'$. This orientation was taken from the VLA maps of Vigotti et al. (1989). Depending on the expected flux density, the total number of such cross-scans was chosen to be between 8 and 64. Individual subscans were checked for interference or residual atmospheric fluctuations and discarded prior to averaging if necessary. We evaluated the differential signals between the main horn and two of the reference horns, which have beam throws of $+3'$ and $-5'$ in azimuth. This allowed a proper judgement of the data quality and enabled us to recognize confusing sources that had been accidentally scanned across by the reference feeds, thus causing a negative response: the probability of picking up unrelated background sources in both reference beams simultaneously is very small so that such a negative response only shows up in one of the two recorded differential signals. The data in the final cross-scans were sampled at $18''$ intervals. With the above scanning speed, this implies an integration time of 0.6 second in each subscan. Averaging also the two scanning directions we obtain a nominal rms noise in the final cross-scans between ~ 2.4 mJy/b.a. (8 scans) and ~ 0.9 mJy/b.a. (64 scans). The actually measured rms

noise values were generally somewhat higher because of residual atmospheric noise. A fit with one Gaussian was applied to the final scan yielding the amplitude, the width, and the position of the centroid of the Gaussian for Stokes parameters I, Q and U. For the double sources with diameters larger than $40''$ we applied a fit with two Gaussians only to the scan along the major axis of the radio source. The decomposition was successful for 74 sources, whose data have S/N larger than 10. As mentioned in the introduction, the linear polarization of the sources will be presented in a future paper. Figure 1 displays some template plots of the cross-scans for sources with different flux densities.

Table 2. Spectral indices for different optical identifications

	N	$\bar{\alpha}$	$\Delta\alpha$
Galaxies on POSS-I	181	-0.837	0.021
Quasars	132	-0.716	0.077
Empty Fields	701	-0.969	0.007

Standard calibration sources were cross-scanned at regular intervals (about every two hours, with two cross-scans each) to check the telescope pointing and flux density scale. For the latter purpose the primary calibrators were 3C 286 and 3C 295, with 3C 48 and 3C 138 being used as secondaries. The pointing accuracy was found to be stable to within $\sim 3''$, sufficiently good to ensure reliable flux density measurements. The exact flux density scale for each target source was applied by checking two subsequent observations of calibration sources. The calibrated flux densities are on the flux density scale of Baars et al. (1977).

In order to recover the total flux the source extension can be used. Therefore we computed the FWHM obtained from the Gaussian fit of the data for point-like sources obtaining the following results: a mean value of $70'' \pm 4''$ for sources stronger than 50 mJy, and for fainter sources $71'' \pm 10''$. The spread of FWHM found permits to recover the total flux with an error of up to 15%. We then decided to determine the integrated flux using a simulation program. The correction factor has been applied to all double and diffuse sources with an angular extent between $20''$ and $40''$ and, in addition, to more extended sources where the deconvolution could not be done because of low S/N.

Our simulation program was built using two point-like components with a flux density ratio R_{20} obtained from the VLA 1.4-GHz maps convolved with the Effelsberg beam (HPBW = $69''$). We had to use R_{20} instead of the unknown flux density ratio of source components at 10.6 GHz ($R_{2.8}$); however, Fig. 4b (see below) will show that $R_{2.8}$ changes by up to a factor of 2. Our simulation shows that this introduces an additional average error of less than 4%.

Another simulation, which takes into account the extended brightness distribution, was used to compute the correction factor for the diffuse sources. The factor for double and diffuse sources is in the range between $\sim 10\%$ and $\sim 35\%$.

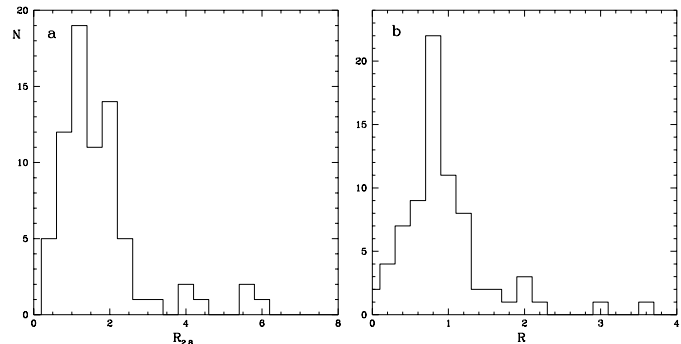


Fig. 4. Histograms of ratios of component flux densities of double sources at a) $\lambda 2.8$ cm, and b) the ratio of the ratios (see text)

2.2. Maps

A total of 53 sources were mapped: they have complex structures larger than $70''$. The map sizes were adjusted such as to ensure sufficient baseline areas and accounting at the same time for the maximum beam throw of the four-feed system, which is $17'$. The standard mapping technique with this receiver system was described by Gregorini et al. (1992). All four horns were employed by observing in the multi-beam mode and applying the restoration algorithm of Emerson et al. (1979). Depending on the strength of the sources, between 2 and 14 coverages were obtained by scanning the telescope in azimuth and separating subsequent scans in elevation by $20''$. After restoration to the equivalent single-beam map the individual coverages were averaged (in I, Q, and U) and then interpolated onto a grid in right ascension and declination. Also in the course of the mapping campaigns standard calibrators were observed and processed in the same way as the target sources. All maps were numerically integrated to yield total flux densities which were also brought to the flux density scale of Baars et al. (1977) by comparison with the mapped flux calibrators. Some of the maps show considerable detail. These will be displayed and briefly described in Sect. 3.

3. Results

3.1. Flux densities at $\lambda 2.8$ cm

The flux densities derived as described in Sect. 2 are compiled in Tab. 1. Column 1 gives the B3 source names, Cols. 2 and 3 the radio centroid (equinox B1950.0) from Vigotti et al. (1989) (computed as the geometric mean

Table 3. B3-VLA Decomposed Double Sources

B3 name	RA (B1950) [^o / ' / "]	DEC (B1950) [h m s]	F(2.8cm) [mJy]	F(20cm) [mJy]	B3 Name	RA (B1950) [^o / ' / "]	DEC (B1950) [h m s]	F(2.8cm) [mJy]	F(20cm) [mJy]
0010+402	00 10 14.3	40 15 52	34.1	150	1016+397	10 17 00.0	39 44 43	4.0	23
	00 10 18.6	40 16 22	15.5	150		10 16 55.0	39 46 07	5.4	28
0015+399	00 15 03.5	40 00 26	24.7	13	1027+383	10 27 43.7	38 18 58	13.6	55
	00 15 03.9	39 59 13	7.3	48		10 27 48.8	38 18 34	18.4	182
0017+432	00 17 26.4	43 13 29	14.5	162	1028+402	10 28 07.2	40 16 36	14.6	137
	00 17 32.3	43 13 33	12.1	84		10 28 07.6	40 15 43	11.4	48
0020+437	00 20 49.7	43 46 13	30.0	233	1040+395	10 40 10.5	39 29 39	25.9	94
	00 20 53.0	43 46 39	14.2	99		10 40 15.9	39 30 22	24.4	119
0146+394	01 46 46.9	39 25 26	9.3	85	1047+396	10 47 20.8	39 41 43	3.4	26
	01 46 47.2	39 23 14	5.8	32		10 47 25.4	39 41 31	2.5	14
0152+435	01 52 25.3	43 30 58	150.8	987	1055+396	10 55 45.8	39 36 54	10.8	42
	01 52 27.2	43 31 43	100.8	522		10 55 57.6	39 34 48	9.1	26
0153+417	01 53 17.6	41 48 10	63.6	243	1105+392	11 05 49.8	39 15 16	109.8	669
	01 53 19.6	41 47 28	36.9	320		11 05 53.9	39 14 35	18.3	90
0159+390	01 59 49.9	39 02 26	10.3	34	1107+379	11 07 02.6	37 54 35	148.0	975
	01 59 53.3	39 02 04	9.8	28		11 07 06.1	37 54 57	145.3	1090
0213+392	02 13 11.1	39 16 56	7.5	42	1109+437	11 09 51.2	43 42 47	48.9	554
	02 13 06.9	39 17 05	6.7	47		11 09 52.8	43 41 56	95.7	634
0216+423	02 15 58.8	42 19 04	79.8	429	1118+390	11 18 28.2	39 01 17	2.5	23
	02 16 03.3	42 19 23	37.4	191		11 18 31.0	38 59 54	4.6	31
0217+417	02 17 04.5	41 43 34	33.1	97	1128+436	11 28 04.9	43 41 10	30.9	271
	02 17 06.5	41 43 50	21.9	32		11 28 05.9	43 42 05	7.5	64
0218+396	02 18 44.9	39 41 18	86.4	404	1141+392	11 41 09.3	39 15 06	15.2	89
	02 18 40.4	39 42 28	70.5	342		11 41 12.4	39 15 37	13.9	71
0218+399A	02 18 44.9	39 55 48	10.0	100	1149+398	11 49 04.7	39 51 25	7.5	40
	02 18 36.5	39 55 01	10.4	101		11 49 12.5	39 50 28	7.8	30
0219+443	02 19 05.1	44 19 57	25.4	112	1222+423	12 21 59.6	42 22 45	60.6	506
	02 19 07.2	44 19 39	38.7	88		12 22 01.6	42 23 33	87.9	636
0221+383	02 21 15.6	38 18 19	9.8	38	1230+398	12 30 16.0	39 53 06	3.1	26
	02 21 08.8	38 18 49	19.0	94		12 30 18.7	39 53 45	5.8	13
0231+391	02 31 43.3	39 10 49	4.1	33	1324+390	13 24 48.3	39 05 56	4.8	25
	02 31 46.9	39 10 23	4.3	37		13 24 47.4	39 04 50	6.6	45
0232+411B	02 32 41.6	41 09 55	93.3	430	1346+392	13 46 47.6	39 15 00	5.9	32
	02 32 50.8	41 10 31	63.3	350		13 46 47.9	39 16 12	7.6	37
0240+404	02 40 22.0	40 29 12	22.5	138	1348+396	13 48 30.4	39 36 35	9.2	40
	02 40 31.6	40 28 45	10.3	30		13 48 32.4	39 35 56	17.4	56
0250+384	02 50 41.2	38 29 50	6.8	159	1349+394	13 49 39.6	39 26 43	7.1	21
	02 50 42.3	38 29 04	23.1	180		13 49 42.9	39 30 20	5.3	16
0700+390	07 00 44.7	39 04 06	10.4	70	1352+397	13 52 00.2	39 42 02	13.9	66
	07 00 32.2	39 04 55	24.5	100		13 52 07.2	39 43 14	2.4	22
0710+457	07 10 49.3	45 45 27	175.1	573	1401+387	14 01 04.6	38 42 50	73.3	290
	07 10 55.3	45 45 12	72.4	300		14 01 05.5	38 41 38	41.2	262
0742+376	07 42 18.8	37 39 13	42.1	427	1410+438	14 10 20.2	43 51 24	22.5	150
	07 42 22.6	37 38 33	42.9	71		14 10 16.4	43 52 25	33.4	208
0759+392	07 59 02.5	39 12 38	6.0	29	1414+398	14 14 30.8	39 51 35	7.6	46
	07 59 03.2	39 13 21	5.7	37		14 14 29.2	39 49 17	3.5	15
0811+391	08 11 04.6	39 09 29	6.9	21	1415+391	14 15 49.9	39 12 11	2.8	11
	08 11 11.2	39 07 37	2.7	53		14 15 52.4	39 11 33	7.4	50
0813+398	08 13 29.6	39 53 46	7.1	45	1436+399	14 36 36.9	39 55 56	2.5	11
	08 13 23.1	39 53 06	9.8	70		14 36 45.5	39 55 50	4.8	23
0824+397	08 24 47.0	39 45 20	12.6	60	1437+427	14 37 50.8	42 46 53	39.7	330
	08 24 50.7	39 46 00	2.2	20		14 37 52.8	42 47 43	16.8	94
0836+402	08 36 54.1	40 15 03	28.7	140	1442+384	14 42 43.5	38 29 52	10.4	53
	08 36 54.4	40 14 14	55.8	395		14 42 37.3	38 29 57	12.6	85
0850+383	08 50 42.1	38 23 06	4.4	32	1444+417A	14 44 28.3	41 45 46	33.3	200
	08 50 40.6	38 22 13	7.6	67		14 44 37.0	41 45 57	38.2	225
0854+399B	08 54 34.0	39 56 18	48.3	234	1446+399	14 46 05.4	39 55 26	3.4	20
	08 54 23.9	39 58 07	22.6	100		14 46 16.1	39 58 08	7.3	50
0905+399	09 05 01.3	39 55 37	11.2	181	1446+440	14 46 40.1	44 04 39	43.3	260
	09 05 10.2	39 55 11	5.7	50		14 46 42.4	44 05 24	26.7	193
0910+392	09 10 39.5	39 14 36	8.4	43	1459+399	14 59 08.1	39 53 49	11.4	38
	09 10 43.7	39 14 35	10.8	60		14 59 21.9	39 55 09	7.2	58
0911+418	09 11 31.7	41 50 09	55.7	226	2304+429	23 04 12.1	42 54 15	25.5	138
	09 11 32.7	41 49 03	58.5	24		23 04 13.8	42 54 52	10.9	116
0918+444	09 18 22.1	44 26 53	68.0	224	2308+393	23 08 34.5	39 22 41	8.2	36
	09 18 09.5	44 26 13	16.6	40		23 08 36.3	39 22 01	6.8	41
0934+387	09 34 48.1	38 45 20	22.7	129	2313+406	23 13 46.9	40 39 24	16.3	127
	09 34 48.2	38 47 08	9.7	65		23 13 47.5	40 38 25	9.2	66
0947+424	09 47 09.3	42 26 54	38.3	251	2330+435	23 30 54.5	43 30 08	4.6	146
	09 47 14.2	42 27 07	21.9	166		23 30 58.2	43 30 17	11.0	88
0951+398	09 51 27.0	39 52 38	12.3	40	2338+393	23 38 47.6	39 20 14	16.2	74
	09 51 27.5	39 51 44	2.7	33		23 38 56.4	39 18 39	19.2	59
0956+391	09 56 41.0	39 12 02	5.6	29	2354+397	23 54 32.7	39 46 53	5.5	35
	09 56 43.8	39 10 51	6.7	29		23 54 36.2	39 45 47	4.6	14

Table 4. B3 VLA sources at 10.6 GHz: the maps

B3 name		RA (B1950) [h m s]	DEC (B1950) [° ' "]	Total flux [mJy]	Comp. flux [mJy]	Dimensions [" × "]	PA [°]	Noise [mJy/beam]
0000+394	N	00 00 08.9	39 31 23.7	17.5	6.5	Point-like		0.8
	S	00 00 09.2	39 28 26.0		11.0	Point-like		
0005+383B		00 05 47.4	38 20 27.4	92.5		60.2 × 33.1	39	0.8
0035+385A		00 35 01.5	38 31 34.1		55.6	Point-like		
0035+385B		00 35 08.2	38 31 14.9	126.9	71.1	22.2 × 4.2	110	0.7
0050+401		00 50 45.2	40 10 54.8		73.8	41.8 × 29.9	5	
0050+402B		00 50 45.4	40 14 58.3	117.4	14.2	Point-like		1.2
0050+403		00 50 45.5	40 18 13.6		29.4	39.5 × 24.0	165	
0115+469	S	01 15 23.6	46 55 39.3		32.3	48.1 × 17.1	23	
	N	01 15 27.2	46 57 14.6	64.3	32.0	Point-like		0.5
0131+390	S	01 31 48.2	39 03 45.0		16.1	22.9 × 13.1	29	
	N	01 31 50.5	39 05 17.5	27.0	10.9	Point-like		0.3
0132+376A		01 32 29.5	37 38 29.8		97.0	43.9 × 37.8	63	
0132+376B		01 32 39.7	37 39 19.6	196.7	99.7	52.5 × 41.3	47	1.7
0157+393B	S	01 57 47.5	39 19 00.0		55.4	124.4 × 57.6	41	
	N	01 57 51.5	39 21 01.2	163.5	108.1	77.2 × 35.4	1	0.9
0157+405A		01 57 01.6	40 36 04.5		49.0*	—		
0157+405B		01 57 49.0	40 33 01.0	94.6*	45.6*	—		1.1
0211+393	W	02 10 57.6	39 18 44.9		14.9	Point-like		
	E	02 11 07.3	39 19 09.5	28.2	13.3	Point-like		0.4
0214+393		02 14 34.0	39 22 36.2	85.5		70.3 × 39.9	37	0.7
0219+428A		02 19 29.8	42 48 31.9	1235.2		51.0 × 9.0	175	3.0
0220+427A		02 20 02.4	42 45 50.9	1806.3*		—		
0221+393	S	02 21 34.3	39 17 57.7		2.3	Point-like		
	N	02 21 37.9	39 20 20.2	7.6	5.3	70.8 × 25.4	104	0.5
0222+403		02 22 37.8	40 18 08.7	182.5		110.3 × 39.9	168	1.3
0225+389		02 25 53.2	38 54 55.3	34.7*		—		1.5
0226+394		02 26 40.9	39 29 57.5	31.3*		—		1.1
0232+411B		02 32 42.0	41 09 59.6		115.6	41.5 × 28.2	75	
0232+411C		02 32 50.3	41 10 32.7	190.1	74.5	35.3 × 21.7	74	1.0
0241+393B	W	02 41 20.1	39 21 02.5		156.7	63.6 × 26.5	62	
	E	02 41 27.0	39 22 06.3	221.3	64.6	39.1 × 21.4	122	0.8
0246+393	W	02 46 59.8	39 22 19.5		207.5	59.7 × 40.9	102	
	E	02 47 10.3	39 22 05.6	380.8	173.3	58.7 × 40.4	85	1.2
0248+467		02 47 38.9	46 44 52.2	379.0*		—		1.1
0258+435		02 58 52.4	43 30 48.0	109.0		Point-like		0.9
	N	07 03 05.2	42 38 33.7		75.2	69.2 × 48.0	127	
0703+426A	C	07 03 10.0	42 36 39.7	608.2	299.8	55.2 × 40.5	148	0.9
	S	07 03 12.0	42 35 08.3		233.2	45.2 × 36.2	20	
0703+426B	N	07 03 30.0	42 38 12.4	71.1	26.7	Point-like		0.9
	S	07 03 30.2	42 36 39.7		44.4	43.1 × 22.8	160	
0709+393	W	07 09 35.6	39 18 51.3		25.9	30.0 × 18.7	3	
	E	07 09 43.9	39 18 17.1	42.6	16.7	Point-like		0.7
0755+379B		07 55 09.4	37 55 17.4	732.3		89.1 × 39.8	109	1.9
0757+395		07 57 32.1	39 33 05.5	27.3*		—		0.7
0831+399	W	08 31 13.0	39 55 31.3		11.1	Point-like		
	E	08 31 21.0	39 54 56.4	16.7	5.6	Point-like		0.9
0834+450A	S	08 34 26.4	45 00 05.6		129.8	50.6 × 29.3	130	
	N	08 34 27.7	45 01 27.7	301.3	171.5	53.6 × 31.7	175	1.2
0843+425	S	08 43 57.5	42 34 07.5		20.4	Point-like		
	N	08 43 59.8	42 35 26.3	51.1	30.7	36.8 × 13.3	13	1.2
0900+389	N	09 00 56.9	38 59 04.1	23.5	16.6	39.4 × 22.4	137	0.8
	S	09 01 01.5	38 57 57.4		6.9	Point-like		
0917+458A	W	09 17 47.0	45 51 02.2		659.4	63.8 × 39.2	43	
	E	09 17 53.9	45 52 44.5	1279.0	619.6	58.9 × 46.3	44	1.9
0938+399B		09 38 17.9	39 58 25.0	341.6		97.5 × 39.7	178	2.8
1013+410	W	10 12 53.0	41 01 43.1		83.8	51.0 × 38.9	88	
	E	10 13 02.9	41 02 02.3	186.3	102.5	59.0 × 44.4	89	1.5
1014+397A	N	10 14 15.4	39 47 29.8	110.2	63.9	121.2 × 43.4	132	1.4
	S	10 14 22.8	39 46 04.6		46.3	81.3 × 40.9	111	
1033+388	S	10 33 41.9	38 50 14.2		16.8	Point-like		
	N	10 33 43.2	38 51 18.6	31.8	15.0	Point-like		0.8
1037+399		10 37 19.3	39 58 07.3	8.6		Point-like		0.8
1154+397		11 54 12.7	39 44 52.1	16.1		109.5 × 36.2	145	0.8
1228+419A		12 28 08.3	41 55 39.8	154.7		140.5 × 69.7	119	1.3
1236+444A	N	12 36 10.6	44 30 20.8	88.8	69.5	Point-like		0.5
	E	12 36 32.6	44 25 09.0		18.8	Point-like		
1236+444B	W	12 36 15.6	44 27 13.8		16.4	Point-like		
	C	12 36 23.3	44 26 11.2	38.7	3.5	Point-like		0.5
1309+412A	S	13 09 26.1	41 12 09.2		52.5	74.8 × 52.8	29	
	N	13 09 28.2	41 17 41.8	116.9	64.4	86.3 × 52.1	179	1.0
1313+387	S	13 13 05.8	38 45 40.5		14.6	Point-like		
	N	13 13 08.4	38 47 22.4	45.8	31.2	30.3 × 14.2	118	1.1
1318+428C		13 18 59.3	42 50 34.5		180.9	62.8 × 35.9	110	
1318+428A		13 19 08.9	42 51 04.3	418.2	237.3	56.1 × 32.8	98	1.2
1330+380	W	13 30 32.0	38 01 20.4		17.6	52.0 × 3.5	116	
	E	13 30 39.8	38 00 18.9	31.7	14.1	Point-like		1.0
1422+395	W	14 22 17.5	39 35 26.0		17.3	49.3 × 9.6	33	
	E	14 22 28.7	39 35 15.6	33.4	16.1	84.8 × 69.7	113	0.6
1447+402		14 47 03.1	40 13 53.4	104.4*		—		0.9
1450+391B		14 50 09.1	39 09 02.7	71.7*		—		0.7
2303+391A	N	23 03 43.0	39 12 05.8	151.1	67.0	44.5 × 22.8	166	0.7
	S	23 03 44.9	39 09 57.8		84.1	64.5 × 26.1	170	
2320+416B		23 20 18.6	41 41 33.1		54.1	26.3 × 6.0	20	
2320+417		23 20 24.2	41 43 03.4	68.1	14.0	Point-like		1.0
2341+396A		23 41 37.2	39 37 18.9	20.3		Point-like		1.4
2341+396B		23 41 43.5	39 35 28.7	22.6*		—		
2351+400B	W	23 51 22.9	40 01 21.8		98.0	58.0 × 36.1	108	
	E	23 51 28.9	40 00 57.9	157.8	59.8	42.6 × 40.5	27	1.6
2354+471		23 54 53.0	47 09 13.2		197.1	70.2 × 46.0	57	
2354+471A		23 55 02.4	47 10 08.2	383.6	186.5	71.7 × 42.2	61	0.9

of the source components). Columns 4 and 5 contain the measured peak (S_{peak}) and integrated (S_{int}) flux densities. The peak flux density was not given for sources that were mapped. When a source was not detected we give an upper limit (marked with a ‘<’ in Col. 5), which corresponds to a $3\text{-}\sigma$ noise computed for the final cross-scan. Column 6 is the updated optical identification. The symbols are g: radio galaxy identified on the POSS-I, most of which are at $z \leq 0.5$; G: far radio galaxy with measured redshift ($0.5 \leq z \leq 3.5$); Q: spectroscopically confirmed quasar; b: blue objects (i.e. non-confirmed quasars); BL: BL Lac; F: featureless spectrum; a blank means ‘empty field’, i.e. it lacks any optical counterpart down to the POSS-I limit (more than 90% are distant radio galaxies, the remaining ones being quasars with magnitudes fainter than the POSS-I). So far the B3-VLA sample is composed of 27% galaxies, 12% quasars, and 61% empty fields. In

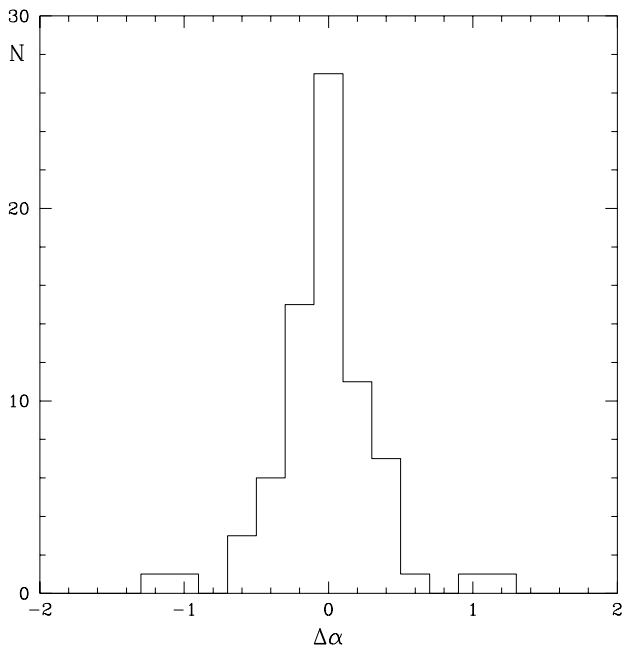


Fig. 5. Histogram of the difference $\Delta\alpha$ between the spectral indices of the two components of double sources

order to have an independent check on the accuracy of our measurements and to evaluate the uncertainties of the flux densities, 143 sources were re-observed. These sources were chosen in different flux bins. Figure 2 shows the plot of the fluxes measured in the two independent observations. Intrinsic source variability increases the scatter of the plot. The analysis of the distribution of the differences between two or more independent flux measurements of the same source allowed for a determination of the random errors affecting the measurements. These errors are the quadratic sum of three terms: the first, proportional to the source intensity, is introduced by gain instabilities of the receiver; the other two, independent of the source flux density, are due to noise and confusion. The first term

was computed using sources with flux densities greater than 500 mJy as well as calibrators, and was found to be $\sim 2\%$. From the faint sources we evaluated the rms noise; we subdivided the sources into different classes according to number of scans (i.e. observing time) and found that this term is in the range 0.6–0.8 mJy. To be conservative we chose 0.8 mJy. For the confusion term we refer to Reich (1993) who reports a value of 0.08 mJy. We expect that the error affecting the flux density measurements is:

$$\sigma_S = \sqrt{(0.02 \cdot S_{\text{tot}})^2 + 0.08^2 + 0.8^2}$$

where S_{tot} is in mJy. To compute the spectral index between 408 MHz and 10.6 GHz (presented in Fig. 3a) the low-frequency flux densities were increased by 5% to adjust them to the scale of Baars et al. (1977). The spectral indices of B30226+394, B30241+393B, B30920+408, B31016+388B, B31428+385, B31447+402, B32333+397, and B32348+387 were not included; the VLA maps show that the components of these triple sources are probably not physically connected.

The spectral indices have a broad distribution with a median value of $\alpha_{\text{med}} = -0.933$ and an average value of $\bar{\alpha} = -0.906$. Figures 3b, 3c, and 3d show the histograms of the spectral indices for three different classes of optical counterparts, i.e. galaxies bright enough to appear on the POSS-I (most of which are at $z < 0.5$), empty fields on the POSS-I (most of which are galaxies $z > 0.5$), and quasars. In Tab. 2 we have compiled the mean spectral indices ($\bar{\alpha}$) and their uncertainties ($\Delta\alpha$) for different optical identifications.

The distributions of the first two classes are similar, but the different average values (see Tab. 2) indicate that high-redshift radio galaxies have steeper spectra. The distribution for quasars shows the presence of two populations: steep-spectrum and flat-spectrum quasars.

For the decomposed double sources (see Sect. 2) Tab. 3 presents in Col. 1 the B3 source names, in Cols. 2 and 3 the positions (equinox B1950.0) of the components from Vigotti et al. (1989); Cols. 4 and 5 give the flux densities at $\lambda 2.8$ cm and $\lambda 20$ cm (Vigotti et al. 1989), respectively. For each source we have computed the component ratio $R_{2.8}$ of the flux density at $\lambda 2.8$ cm (see Fig. 4a), and the ratio R_{20} of the flux density at $\lambda 20$ cm, then the ratio $R = R_{2.8}/R_{20}$ (see Fig. 4b). These ratios were computed considering as the first component the brightest one at 20 cm. Figure 4a shows that the double sources at $\lambda 2.8$ cm are symmetric with respect to the flux densities; in fact only 18% have a ratio greater than 2 (very high values could also be an indication that the two components are not physically connected). Figure 4b shows that only 10% of double sources change their flux density ratio between 1.4 and 10.6 GHz by more than a factor of 2.

The spectral index computed between $\lambda 20$ cm and 2.8 cm for the single components has a median value of -0.890 . Figure 5 presents the difference $\Delta\alpha$ between the

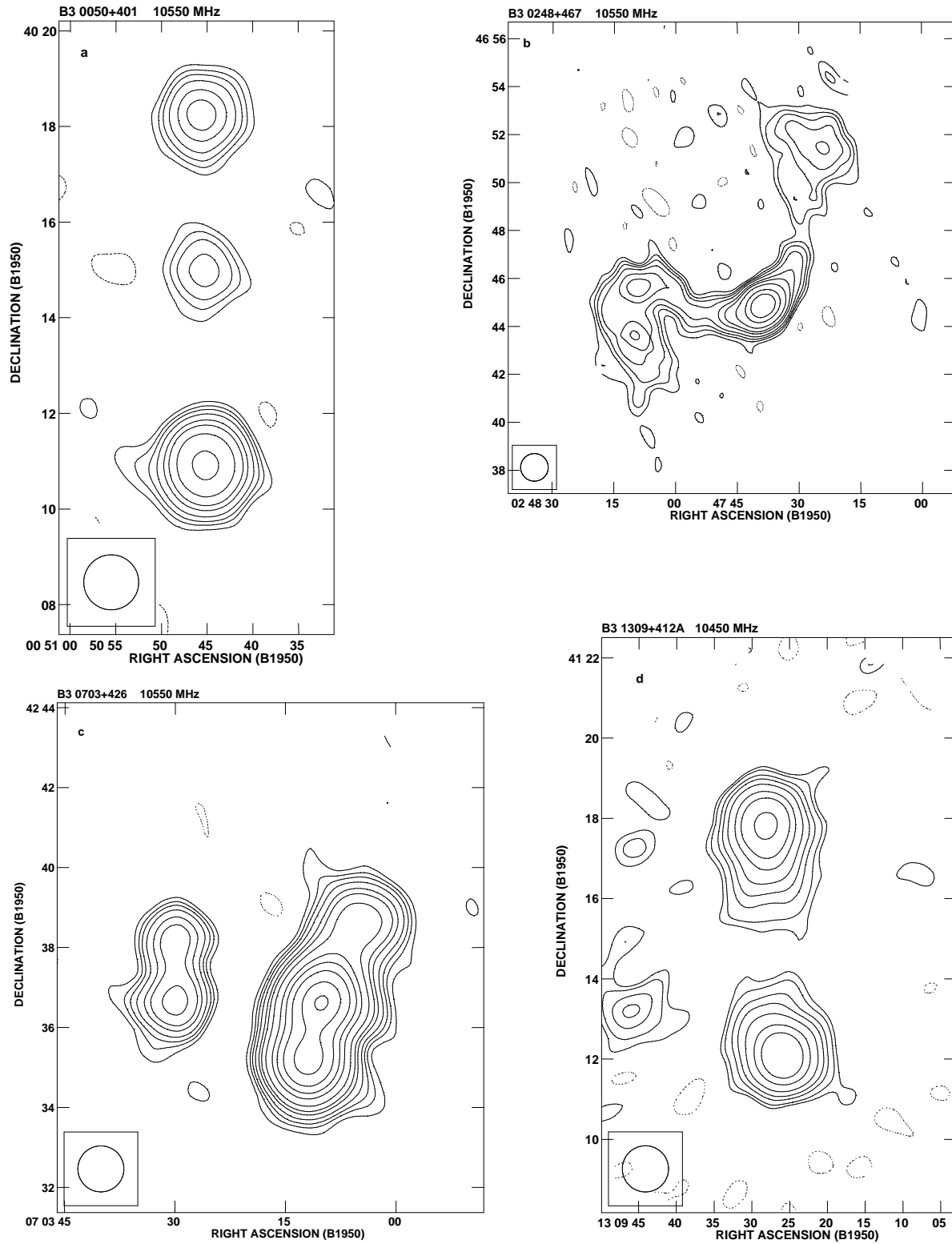


Fig. 6. Maps of four B3 sources with complex structure at $\lambda 2.8$ cm: a) B3 0050+401 – contour levels: -3, 3, 5, 7, 10, 15, 20, 30, 50 mJy ; b) B3 0248+467 – contour levels: -3, 3, 5, 7, 10, 15, 20, 30, 50, 70, 100, 150, 200 mJy; c) B3 0703+426 – contour levels: -3, 3, 5, 7, 10, 15, 20, 30, 50, 70, 100, 150, 200 mJy; d) B3 1309+412A – contour levels: -2, 2, 3, 5, 7, 10, 15, 20, 30 mJy

spectral indices of the two components of the 74 double sources. The distribution of $\Delta\alpha$ is asymmetric, in the sense that source components that are brighter at $\lambda 20$ cm exhibit slightly steeper spectra on average.

The parameters of the mapped sources are presented in Tab. 4. Column 1 gives the B3 source names, Col. 2 a letter which marks the component. All the parameters presented in Cols. 3 through 8 are determined with a two-dimensional Gaussian fit to the $\lambda 2.8$ cm data. Columns 3 and 4 contain the component positions (equinox B1950.0); Cols. 5 and 6 give the integrated flux of the whole source and of the components, respectively; Cols. 7 and 8 have the FWHM and position angle. Column 9 gives the noise of the map. For complex sources, not well approximated by a Gaussian, the total flux densities are marked with an asterisk. Note that the rms noise in the maps is comparatively low with respect to the cross-scans. This is due to the fact that in mapping all four horns have been used, while in the cross-scans only the main beam was measuring the target, and the offset feeds were used to reject atmospheric noise. It is clear that the reference feeds add uncorrelated noise to the differential signal in the cross-scans, whereas in case of mapping they contribute to the source flux density measurement. In Fig. 6 we show five maps of those sources that exhibit the most complex structure at this resolution.

3.2. Notes on individual mapped sources

- *B3 0050+401*: This is a triple source consisting of a core and two lobes. The core has an inverted spectrum ($\alpha = 0.64$) between 1.465 and 10.6 GHz. Note that there is an error in Tab. II of Vigotti et al. (1989), which gives 111 mJy for the core at 1.465 GHz, while this should be 4 mJy. The source has a total spectral index $\alpha = -0.719$ between 0.408 and 10.6 GHz (Fig. 6a).
- *B3 0157+393*: This one is reminiscent of wide-angle tailed sources. The brightness asymmetry visible at 1.465 GHz (Vigotti et al. 1989) is also visible at 10.6 GHz. The spectrum is relatively flat ($\alpha = -0.59$) between 408 MHz and 10.6 GHz, indicating that the core may contribute proportionally more at the high frequency.
- *B3 0157+405*: This turns out to be a giant radio galaxy (Schoenmakers, priv. comm.). The spectrum is steep ($\alpha = -1.18$) between 0.408 and 10.6 GHz, indicating significant particle ageing. This is in line with the rather relaxed radio continuum morphology seen at both frequencies, and with the lack of any core and jets.
- *B3 0220+427*: This is 3C 66: between 408 MHz and 10.6 GHz the spectrum of the compact source B3 0219+428A (3C66A) is relatively flat ($\alpha = -0.432$), the radio source B3 0220+427A/D is a FRI with $\alpha = -0.646$.

- *B3 0248+467*: An S-shaped radio galaxy identified with IC260. At 10.6 GHz the core becomes very prominent. The total spectral index between 0.408 and 10.6 GHz is $\alpha = -0.57$ (Fig. 6b).
- *B3 0703+426*: The map contains two sources: B3 0703+426A and B3 0703+426B. The first, identified with a cluster galaxy, has $\alpha = -0.60$ (between 0.408 and 10.6 GHz); the second, identified with a compact object, has $\alpha = -0.82$ (Fig. 6c).
- *B3 1309+412A*: A FRII radio galaxy; the spectral index was not computed because the 408 MHz flux density also includes B3 1309+413 (Fig. 6d).
- *B3 1450+391*: A very diffuse radio source probably identifiable with a cluster galaxy. The spectrum is steep ($\alpha = -0.97$); however, the flux densities at 408 MHz and at 10.6 GHz can be underestimated.

Acknowledgements. We are grateful to H. Rottmann and G. Zech for their invaluable help during the many observing runs. We wish to thank our referee, Dr. J.J. Condon, for his useful comments. Part of this work was supported by the Deutsche Forschungsgemeinschaft, grant KL533/4-2, and by the European Commission, TMR Programme, Research Network Contract ERBFMRXCT97-0034 “CERES”. We thank Dr. H. Andernach for a careful check of the tables.

References

- Baars J.W.M., Genzel R., Pauliny-Toth I.I.K., Witzel A., 1977, *A&A* 61, 99
- Condon J.J., Cotton W.D., Greisen E.W., Yin Q.F., Perley R.A., Taylor G.B., Broderick J.J., 1998, *AJ* 115, 1693
- Emerson D.T., Klein U., Haslam C.G.T., 1979, *A&A* 76, 92
- Ficarra A., Grueff G., Tomassetti G., 1985, *A&AS* 59, 255
- Gregory P.C., Scott W.K., Douglas K., Condon J.J., 1996, *ApJS* 103,427
- Gregorini L., Klein U., Parma P., Schlickeiser R., Wielebinski R., 1992, *A&AS* 94, 13
- Hales S.E.G., Baldwin J.E., Warner P.J., 1988, *MNRAS* 234, 919
- Kapahi V.K., Kulkarni V.K., 1986, *A&A* 165, 39
- Kulkarni V.K., Mantovani F., 1985, *A&A* 153, 13
- Kulkarni V.K., Mantovani F., Pauliny-Toth I.I.K., 1990, *A&AS* 82, 41
- Kühr H., Witzel A., Pauliny-Toth I.I.K., Nauber U., 1981, *A&AS* 45, 367
- Reich W., 1993, in: *Effelsberg News* 2, MPIfR Bonn
- Rengelink R., Tang Y., de Bruyn A.G., Miley G.K., Bremer M.N., Röttgering H.J.A., Bremer M.A.R., 1997, *A&AS* 124, 259
- Vigotti M., Grueff G., Perley R., Clark B.G., Bridle A.J., 1989, *AJ* 98, 419